

Improved High Voltage Electrochemical Stability of Single-Crystal $\text{LiNi}_{0.5}\text{Co}_{0.2}\text{Mn}_{0.3}\text{O}_2$ by Mg-Fe Co-Doped Li_3AlF_6 Coating

Boyu Liu, Qing Pang, Tengfei Wang, Xiufen Li, and Hongyu Wang*

The single-crystal $\text{LiNi}_{0.5}\text{Co}_{0.2}\text{Mn}_{0.3}\text{O}_2$ (NCM523) offers a substantial theoretical specific capacity along with outstanding cycle stability. Despite the superior stability of the single-crystal structure compared to its polycrystalline counterpart, the NCM523 single-crystal material may experience structural changes, such as oxygen release and transition metal dissolution, under high-voltage conditions (greater than 4.3 V). These changes can lead to capacity decay or battery failure. Enhancing the electrochemical performance of single-crystal NCM523 under high-voltage conditions is crucial for advancing lithium-ion battery performance. In this work, a Mg-Fe co-doped Li_3AlF_6 -coated single-crystal NCM523 material via a liquid-phase method is prepared.

The Mg-Fe co-doped Li_3AlF_6 -coated NCM523 exhibits excellent electrochemical properties at a voltage of 4.5 V, reaching a specific discharge capacity of 215.5 mAh g^{-1} . Following 200 cycles at 1 C, the retention rate is 91.33%, significantly outperforming the original NCM523, which shows a capacity of $178.84 \text{ mAh g}^{-1}$ and a retention ratio of 44.16%. The co-doping of Mg and Fe enhances the conductivity of Li_3AlF_6 . The stability of the material under high voltage is enhanced by this modified coating, which also lowers its charge transfer resistance. This research provides important perspectives for developing high-performance cathode materials for lithium-ion batteries.

1. Introduction

Lithium-ion batteries have garnered significant consideration as energy storage devices because of their high energy density and impressive coulombic efficiency.^[1] The cathode material is crucial to the efficiency of lithium-ion batteries, as it significantly affects their electrochemical properties.^[2] Among the various options, single-crystal $\text{LiNi}_{0.5}\text{Co}_{0.2}\text{Mn}_{0.3}\text{O}_2$ (NCM523) is perceived as a promising cathode for advanced batteries, primarily on account of its high energy density and excellent cycle stability.^[3] However, enhancing the energy density of NCM523 remains a significant challenge. While increasing the operating voltage presents a viable approach, it also results in the release of lattice oxygen and the dissolution of transition metals, which can diminish its capacity.^[4,5] To enhance the electrochemical performance of NCM523 at elevated voltages, researchers have explored modifications to the electrolyte and employed various strategies, such as doping and coating strategies, to keep its lattice structure stable and suppress the dissolution and side reactions of transition metals.

Among various modification strategies, the surface coating method has garnered significant attention due to its ability to directly isolate the cathode and the electrolyte. This separation effectively retards interface structural degradation and inhibits side reactions.^[6] However, traditional coating materials, such as metal oxide coatings, are electrochemically inert, potentially

hindering the improvement of both the cathode material's capacity and the transmission of lithium ions.^[7] Therefore, numerous researchers have started to investigate materials that can maintain stable electrochemical performance under high-voltage conditions as coating layers, such as metal phosphate and metal fluoride coating layers.^[8,9] A notable example is LiF coating, which is a major component of the cathode-electrolyte interface (CEI) membrane. It can inhibit side reactions during cycling and exhibit excellent electrochemical stability in the voltage range of 0–6.4 V.^[10] This characteristic significantly enhances the material's ability to withstand high voltages. Nevertheless, its ionic conductivity requires further enhancement. Recent studies indicate that ternary lithium fluoride materials, such as LiAlF_4 and Li_3AlF_6 , fulfill these requirements due to their wide voltage window and excellent Li^+ conductivity.^[11,12] Therefore, research is also being conducted on their application as coatings for cathode materials. Hiroaki^[13] prepared Li_3AlF_6 -coated LiCoO_2 and $\text{LiNi}_{0.5}\text{Mn}_{1.5}\text{O}_4$. The modified LiCoO_2 and $\text{LiNi}_{0.5}\text{Mn}_{1.5}\text{O}_4$ demonstrated discharge capacities of 170 mAh g^{-1} and 146.5 mAh g^{-1} at high voltages of 4.5 V and 5 V, respectively. The enhanced discharge capacity of the modified materials surpassed that of their unmodified counterparts, and the capacity retention rates after cycling were also improved (95.8% vs 63.2% for LiCoO_2 and 98.2% vs 94.2% for $\text{LiNi}_{0.5}\text{Mn}_{1.5}\text{O}_4$). Jin^[14] prepared LiAlF_4 -coated NCM811 material, which maintained a capacity of 140 mAh g^{-1} after 300 cycles within the voltage range from 2.75 to 4.5 V. The capacity attenuation was slower than that of the unmodified material, which experienced a rapid decline to below 140 mAh g^{-1} after several cycles. These studies collectively demonstrate that metal fluoride-based coatings can stabilize the interface without compromising the electrochemical performance of the materials. Notably,

B. Liu, Q. Pang, T. Wang, X. Li, H. Wang
Qinghai Provincial Key Laboratory of New Light Alloys
Qinghai University
Xining 810016, P. R. China
E-mail: wanghongyu@qhu.edu.cn

Li_3AlF_6 is identified as a more suitable coating material due to its voltage window of 6.48 V and superior phase stability.^[15] Although the ionic conductivity of Li_3AlF_6 has significantly improved compared to LiF , its electronic conductivity remains low. To improve the material's overall conductivity and enhance its electrochemical performance, a viable strategy involves doping and modifying the material.^[16,17] However, research on further modifying Li_3AlF_6 and utilizing it as a coating layer for high-voltage cathode materials is still lacking.

In this study, Mg-Fe co-doped Li_3AlF_6 was successfully coated on single-crystal NCM523 using a liquid-phase method and a simple calcination process. Considering the similar ionic radii of Mg^{2+} (0.072 nm) and Fe^{3+} (0.064 nm), both ions were chosen for co-doping into Li_3AlF_6 in this study.^[18,19] The effects of single-element doping and Mg-Fe co-doping on the electrochemical properties of the Li_3AlF_6 coating layer applied to single-crystal NCM523 were compared. The results indicate that Mg-Fe co-doping shows superior performance compared to single-element doping, demonstrating a significant modification effect. Furthermore, the cathode performance of Mg-Fe co-doped samples with different coating content was also studied. As the coating content increased, the polarization phenomenon of the cathode material also increased, leading to a decline in electrochemical performance. When 1 wt% Mg-Fe co-doped modified Li_3AlF_6 was utilized as the coating material, the modified NCM523 exhibited optimal electrochemical performance, tested at a high voltage of 4.5 V. At a rate of 0.1 C, the capacity reached 215.5 mAh g⁻¹, and after 200 cycles at 1 C, the discharge-specific capacity reached 148.1 mAh g⁻¹, with a retention rate of 91.33%, higher than that of the unmodified sample (44.16%). The finding offers significant guidance for advancing premium lithium-ion batteries.

2. Results and Discussion

Figure 1 provides a schematic overview of the synthesis process. By dispersing single-crystal NCM523 in the mixed solution, the modified material is obtained after heat treatment. Initially, Figure S1, Supporting Information presents the XRD patterns of the solely synthesized Li_3AlF_6 (LAF) and $\text{Li}_3\text{AlF}_6\text{-Mg-Fe}$ (LAF-Mg-Fe), indicating that the diffraction peaks of both materials match PDF card number 88-0860, which is associated with the structure of Li_3AlF_6 . This observation demonstrates that the doped elements do not influence the formation of the Li_3AlF_6 phase. The (310) peak position of the doped LAF-Mg-Fe sample shifted compared to that of LAF. Furthermore, Figure 2a displays the XRD patterns of NCM523, NCM523-LAF-1, and NCM523-LAF-Mg-Fe-1. The diffraction peaks of all samples relate to PDF card number 74-0919. The narrow and sharp peaks indicate high crystallinity in all samples.^[20] The $\alpha\text{-NaFeO}_2$ layered structure, which belongs to the $R\bar{3}m$ space group is responsible for these peaks. The unique crossover peaks observed at (006)/(012) and (108)/(110) further demonstrate that all materials possess a well-ordered layered structure.^[21] To quantify the $\text{Li}^+/\text{Ni}^{2+}$ mixing degree, GSAS Rietveld software was used for phase refinement, as shown in Figure 2b-d and Table 1. Since the refined R_{wp} values fall within the acceptable range, the results of the refinement can be considered reliable.^[22] Initially, each sample exhibited a c/a ratio exceeding 4.9, which is indicative of an ordered structure in all samples. The refined results indicate that the NCM523-LAF-Mg-Fe-1 sample exhibits the lowest degree of $\text{Li}^+/\text{Ni}^{2+}$ mixing at 3.24%, suggesting that the LAF-Mg-Fe coating effectively reduces cation mixing. This observation aligns with the I(003)/(104) values presented in Table 1, where the NCM523-LAF-Mg-Fe-1 sample displays the highest ratio; a larger ratio signifies a

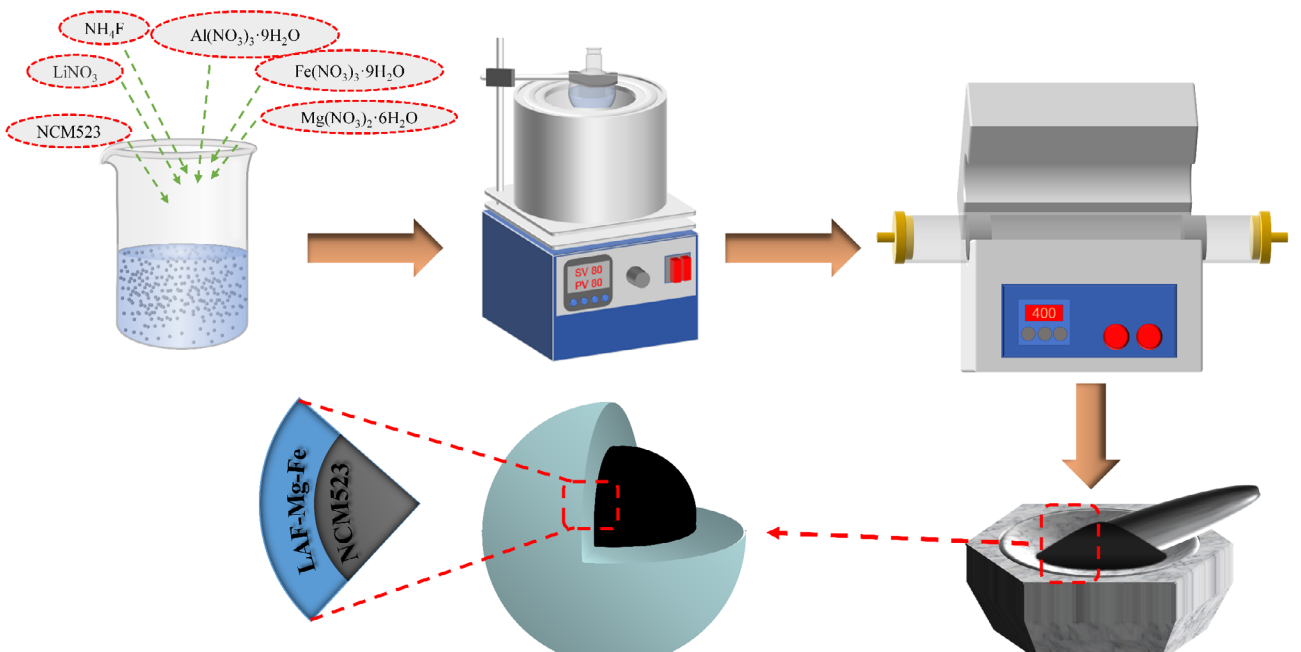


Figure 1. The schematic diagram of the preparation process of $\text{Li}_3\text{AlF}_6\text{-Mg-Fe}$ -coated NCM523.

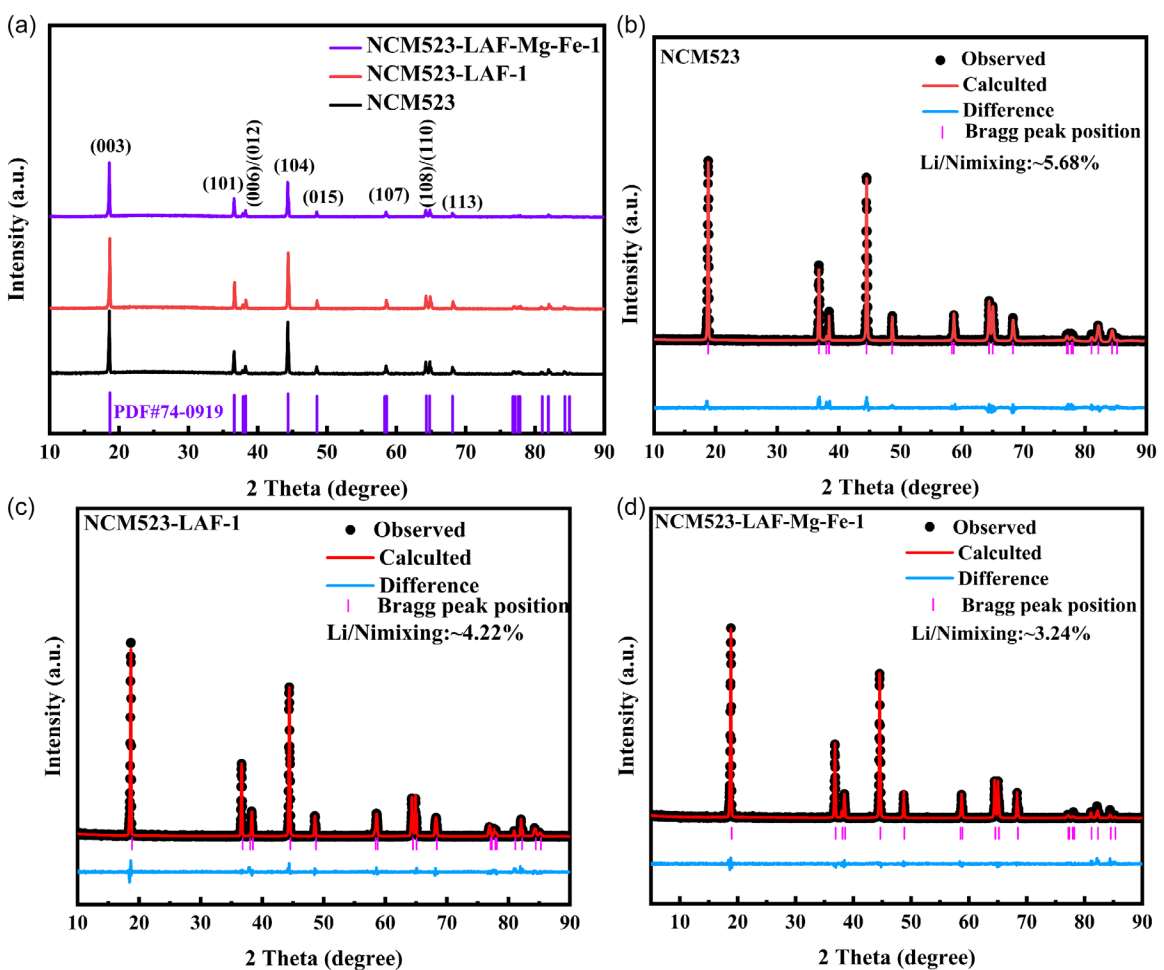


Figure 2. a) XRD patterns of NCM523, NCM523-LAF-1, and NCM523-LAF-Mg-Fe-1. b-d) GSAS Rietveld refinement results.

Table 1. Rietveld refinement data of XRD patterns of NCM523, NCM523-LAF-1 and NCM523-LAF-Mg-Fe-1.					
Sample	a [Å]	c [Å]	c/a	$I[003]/I[104]$	R_{wp} [%]
NCM523	2.87540	14.24202	4.95306	1.15	3.52
NCM523-LAF-1	2.87146	14.25453	4.96421	1.22	2.98
NCM523-LAF-Mg-Fe-1	2.87478	14.25950	4.96020	1.25	2.43

lower degree of cation disorder.^[23] Furthermore, the XRD patterns and unit cell parameters of the NCM523-LAF-Mg-1 and NCM523-LAF-Fe-1 samples, as well as the NCM523-LAF-Mg-Fe-2 and NCM523-LAF-Mg-Fe-3 samples, were analyzed, as illustrated in Figure S2a,b and Table S1, Supporting Information. By comparing the $I(003)/(104)$ values of the samples doped with either Mg or Fe and those co-doped with Mg-Fe at varying doping levels, it is evident that the NCM523-LAF-Mg-Fe-1 sample continues to exhibit a higher value, indicating that the LAF-Mg-Fe modified coating with a 1% coating amount effectively mitigates the degree of $\text{Li}^{+}/\text{Ni}^{2+}$ cation mixing.

Figure 3 reveals the SEM images of the NCM523 samples (Figure 3a-c), along with the NCM523-LAF-1 (Figure 3d-f) and

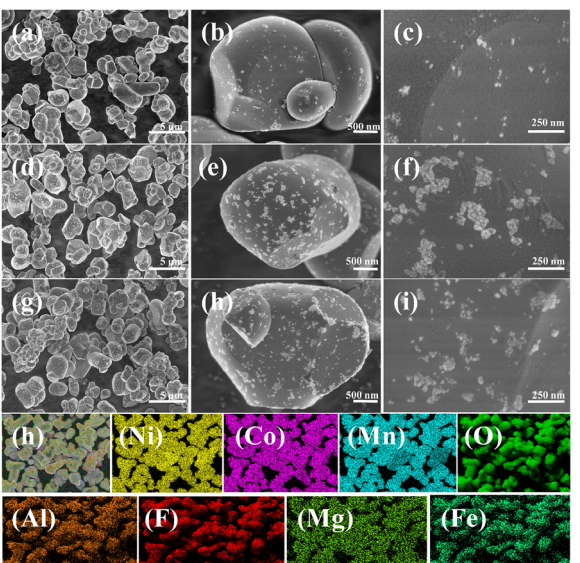


Figure 3. SEM images of a-c) NCM523. d-f) NCM523-LAF-1, and g-i) NCM523-LAF-Mg-Fe-1. h) EDS elemental mapping of NCM523-LAF-Mg-Fe-1.

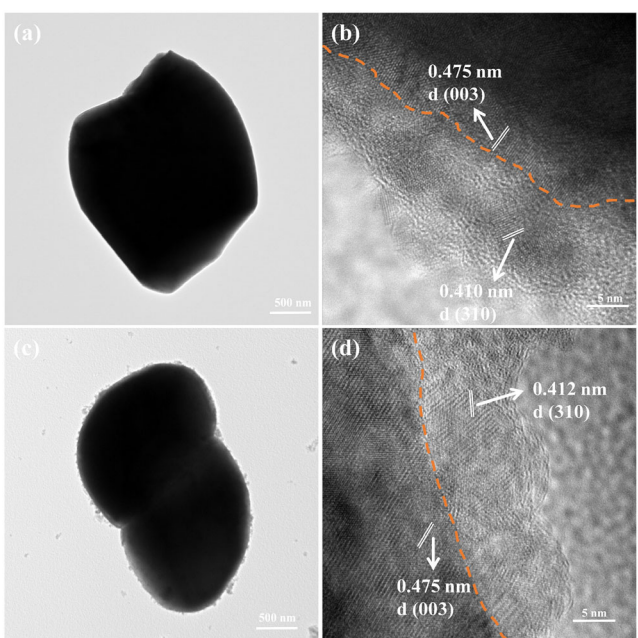


Figure 4. TEM and HRTEM images of a,b) NCM523-LAF-1 and c,d) NCM523-LAF-Mg-Fe-1.

NCM523-LAF-Mg-Fe-1 (Figure 3g–i) samples. Additionally, Figure S3, Supporting Information displays NCM523-LAF-Mg-Fe-2 (Figure S3a–c, Supporting Information) and NCM523-LAF-Mg-Fe-3 (Figure S3d–f, Supporting Information) samples. All samples exhibit a comparable single-crystal particle morphology.

Following the surface coating with LAF or LAF-Mg-Fe, the surface topography of NCM523 changed noticeably, resulting in a blurred appearance. As the coating loading of LAF-Mg-Fe increased, the degree of surface blurring increased gradually. To investigate the elemental distribution in the NCM523-LAF-Mg-Fe-1 sample, the energy-dispersive spectroscopy (EDS) image was obtained, as illustrated in Figure 3h. The results demonstrated that Ni, Co, Mn, O, Al, F, Mg, and Fe were evenly spread across the particle surface. Figure 4 showcases the TEM and HRTEM images of the NCM523-LAF-1 and NCM523-LAF-Mg-Fe-1 samples, with Figure 4a,b representing NCM523-LAF-1 and Figure 4c,d representing NCM523-LAF-Mg-Fe-1. A coating \approx 15 nm thick can be observed on the surface of both samples. The lattice fringe spacings of 0.410 nm and 0.412 nm are attributed to the (310) crystal face of Li_3AlF_6 , while the lattice fringe spacing of 0.475 nm is associated with the (003) crystal face of NCM523. Notably, the interplanar spacing of the coating layer in the NCM523-LAF-Mg-Fe-1 sample exhibits a certain increase compared to that in the NCM523-LAF-1 sample, which may be attributed to the co-doping with Mg and Fe in the bulk phase of Li_3AlF_6 . The expanded interlayer spacing provides wider channels for Li-ions, thereby reducing the diffusion resistance.

Figure 5 presents the X-ray photoelectron spectroscopy (XPS) analysis of the surface elemental valence states of different samples. Figure 5a shows the Ni fine spectra of NCM523, NCM523-LAF-1, and NCM523-LAF-Mg-Fe-1. The Ni spectra display two Ni 2p peaks accompanied by two satellite peaks, with the electron binding energy for Ni 2p_{3/2} observed at 855.4 eV and that for Ni 2p_{1/2} at 872.4 eV.^[24] By fitting the Ni 2p_{3/2} peak, the ratio of Ni²⁺ to

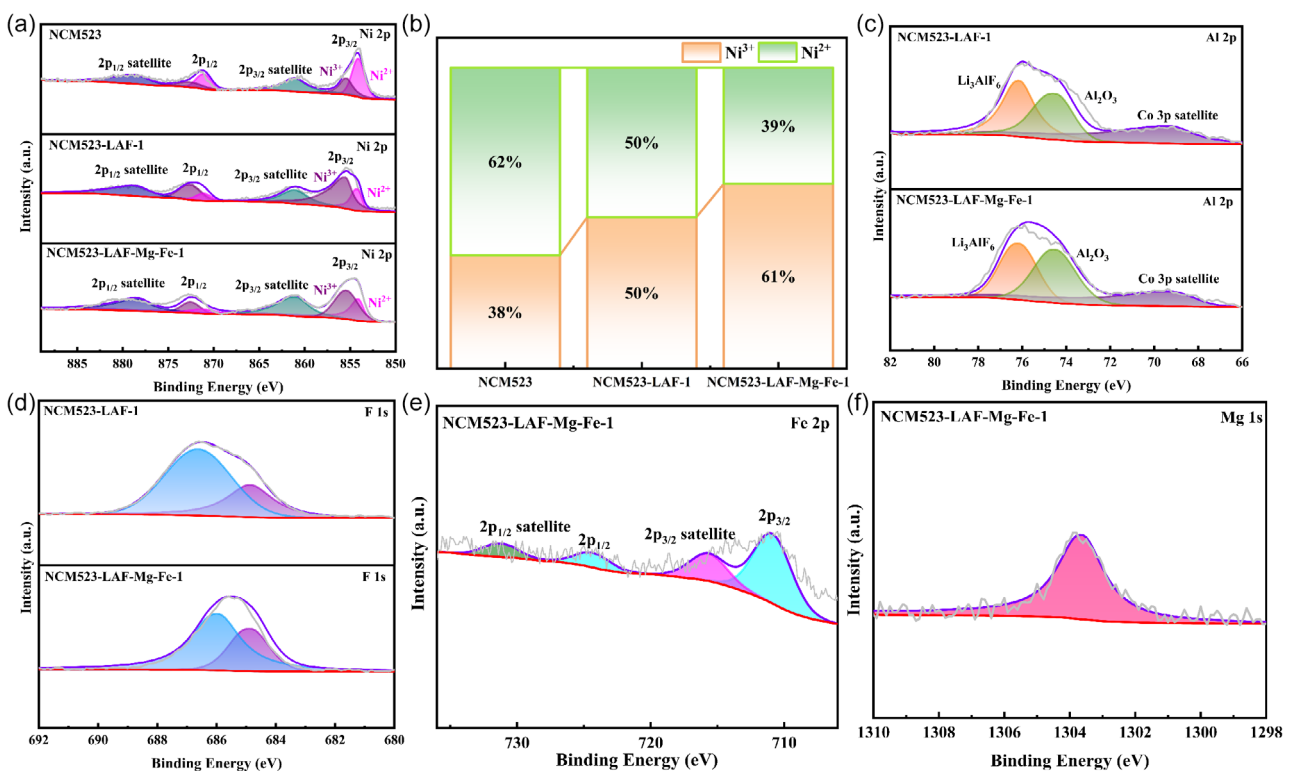


Figure 5. XPS spectra of a) Ni 2p and b) Ni²⁺/Ni³⁺ ratio for NCM523, NCM523-LAF-1, and NCM523-LAF-Mg-Fe-1. c) Al 2p. d) F 1s for NCM523-LAF-1 and NCM523-LAF-Mg-Fe-1. e) Fe 2p and f) Mg 1s for NCM523-LAF-Mg-Fe-1.

Ni^{3+} can be determined, as depicted in Figure 5b. The results show Ni^{2+} proportions of 62%, 50%, and 39% for NCM523, NCM523-LAF-1, and NCM523-LAF-Mg-Fe-1, respectively. Observations indicate that the LAF-Mg-Fe coating, relative to the undoped LAF, more effectively diminishes $\text{Li}^+/\text{Ni}^{2+}$ cation mixing, which helped enhance the electrochemical performance. Figure 5c shows the Al 2p spectra of NCM523-LAF-1 and NCM523-LAF-Mg-Fe-1. Notably, the Co 3p peak can be observed at 69.7 eV.^[25] The peak at 75.8 eV corresponds to Li_3AlF_6 , while another peak at 74.5 eV corresponds to Al_2O_3 .^[26] The F 1s spectra of NCM523-LAF-1 and NCM523-LAF-Mg-Fe-1 are shown in Figure 5d. Compared with NCM523-LAF-1, the F 1s peak of NCM523-LAF-Mg-Fe-1 shifts to lower binding energy. This shift is attributed to the electron transfer at the cathode-coating interface in the LAF-Mg-Fe coating sample.^[27] Additionally, XPS analysis was conducted on the LAF and LAF-Mg-Fe samples, and the results for the F 1s peaks are presented in Figure S4, Supporting Information. It is evident that, compared to the F 1s peak of the LAF-Mg-Fe sample, the F 1s peak of LAF also shifted toward lower electron binding energy. Moreover, as depicted in Figure 5e,f, the Fe 2p peak at \approx 711.1 eV and the Mg 1s peak at around 1303.6 eV demonstrate the existence of Mg and Fe components on the surface of the NCM523-LAF-Mg-Fe-1 sample.^[28,29]

The samples were fabricated into electrodes to evaluate their electrochemical efficiency. The charge-discharge curves for three samples: NCM523, NCM523-LAF-1, and NCM523-LAF-Mg-Fe-1, are presented in Figure 6a, which spans a voltage range from 3.0 to 4.5 V. The discharge-specific capacities at 0.1 C are 178.92 mAh g⁻¹ for NCM523, 195.21 mAh g⁻¹ for NCM523-LAF-1, and 213.12 mAh g⁻¹ for NCM523-LAF-Mg-Fe-1, respectively.

Figure S5a,b, Supporting Information present the charge-discharge curves for the single-element doped samples NCM523-LAF-Mg-1 and NCM523-LAF-Fe-1, as well as the samples with different coating loadings, NCM523-LAF-Mg-Fe-2 and NCM523-LAF-Mg-Fe-3. A comprehensive comparison indicates that the co-doped sample NCM523-LAF-Mg-Fe-1, which has a lower coating amount, exhibits the highest discharge-specific capacity. This enhancement can be attributed to the modified LAF-Mg-Fe coating layer, which improves the electrode's discharge capacity, while the incorporation of Mg and Fe further boosts the charge-discharge efficiency of the electrode. Notably, as the coating amount increases, the discharge capacity decreases gradually, suggesting that a higher coating amount of LAF-Mg-Fe adversely affects the capacity of the modified NCM523.

Figure 6b illustrates the rate capability plots of three samples: NCM523, NCM523-LAF-1, and NCM523-LAF-Mg-Fe-1, at rates of 0.2 C, 0.5 C, 1 C, 2 C, and 5 C. Additionally, Figure S5c,d, Supporting Information present the rate capability plots for NCM523-LAF-Mg-1, NCM523-LAF-Fe-1, NCM523-LAF-Mg-Fe-2, and NCM523-LAF-Mg-Fe-3. Notably, at a high rate of 5 C, the specific capacities observed are 84.12 mAh g⁻¹ for NCM523, 118.22 mAh g⁻¹ for NCM523-LAF-1, and 124.84 mAh g⁻¹ for NCM523-LAF-Mg-Fe-1. Upon returning to a rate of 0.2 C, all samples demonstrate recovery of discharge-specific capacities to values close to the initial 0.2 C specific capacity, indicating that the structural integrity of the samples remains largely intact and that they exhibit commendable structural stability. The data reveal that the NCM523 sample coated with 1% LAF-Mg-Fe displays superior rate performance compared to both the initial

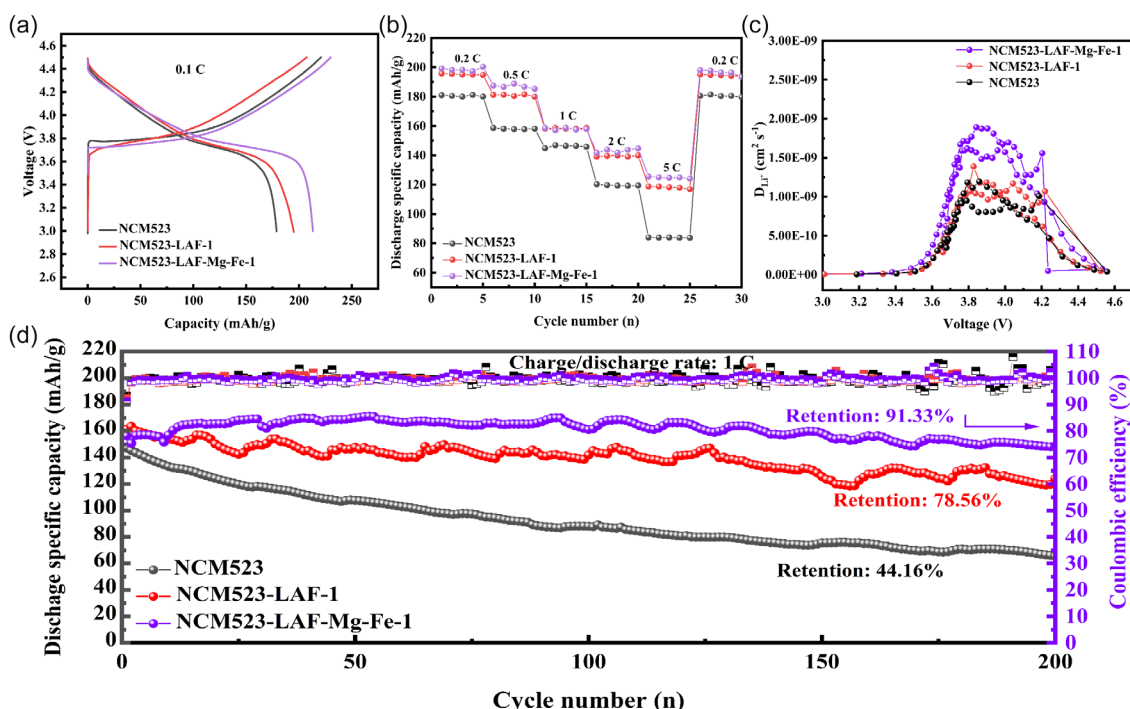


Figure 6. Electrochemical performance of NCM523, NCM523-LAF-1, and NCM523-LAF-Mg-Fe-1 samples: a) Charge-discharge curves. b) Rate capability. c) Li^+ diffusion coefficients, and d) cycling stability.

NCM523 and pure LAF-coated NCM523. This enhancement can be attributed to the co-doped modified LAF-Mg-Fe coating layer, which confers greater stability and higher ionic conductivity to the battery compared to the LAF coating alone. Furthermore, an evaluation of the rate performance of the samples depicted in Figure S5c,d, Supporting Information under identical conditions further substantiates that the NCM523 material coated with LAF containing a minor amount of co-doped Mg and Fe exhibits enhanced rate performance compared to samples with single-element doping.

Figure 6c shows the lithium-ion diffusion coefficients in NCM523, NCM523-LAF-1, and NCM523-LAF-Mg-Fe-1 samples measured using the GITT method. The test results are calculated according to Formula (1).^[30]

$$D^{\text{GITT}} = \frac{4}{\pi\tau} \left(\frac{m_B V_M}{M_B S} \right)^2 \left(\frac{\Delta E_s}{\Delta E_t} \right)^2 \quad (1)$$

The Li⁺ diffusion coefficient (D^{Li^+}) was obtained by the equation involving key parameters: m_B (mass of active material), M_B (molecular weight), V_M (molar volume), S (electrode area), τ (duration of single current pulse), ΔE_s (steady-state voltage difference measured after 30-min relaxation period), and ΔE_t (transient voltage difference following current pulse application). As shown in Figure 6c, the NCM523-LAF-Mg-Fe-1 sample exhibits significantly higher Li⁺ diffusion coefficients during the initial charge-discharge cycle compared to both pristine NCM523 and NCM523-LAF-1 samples. This is explained by the expanded interlayer spacing of the coating layer, which promotes Li⁺ transport. Notably, when contrasted with the samples presented in Figure S6a,b, Supporting Information the co-doped sample with 1% coating content also demonstrates superior diffusion coefficients over those of single-element doped counterparts and high-coating-content samples. These results collectively confirm that the 1 wt% LAF-Mg-Fe composite coating effectively reduces the diffusion energy barrier, as evidenced by the enhanced lithium-ion transport kinetics.

Figure 6d presents the cycling performance of NCM523, NCM523-LAF-1, and NCM523-LAF-Mg-Fe-1 samples after 200 cycles at 1 C. The pristine NCM523 exhibits a capacity retention of 44.16% (66.02 mAh g⁻¹), while NCM523-LAF-1 and NCM523-LAF-Mg-Fe-1 demonstrate significantly improved retentions of 78.56% (121.36 mAh g⁻¹) and 91.33% (148.12 mAh g⁻¹), respectively. Notably, the co-doped NCM523-LAF-Mg-Fe-1 outperforms all other samples in long-term cycling stability. Furthermore, as illustrated in Figure S6c,d, Supporting Information the cycling performance of single-doped samples (NCM523-LAF-Mg-1 and NCM523-LAF-Fe-1) and high-coating-content samples (NCM523-LAF-Mg-Fe-2 and NCM523-LAF-Mg-Fe-3) was evaluated under identical conditions. Their capacity retentions are 80.64% (116.05), 81.85% (125.06), 71.44% (106.42 mAh g⁻¹), and 66.13% (102.88 mAh g⁻¹), respectively, all of which are inferior to that of the 1% LAF-Mg-Fe-coated NCM523-LAF-Mg-Fe-1. These findings further indicate that, compared to LAF, the LAF-Mg-Fe coating enhances its conductivity as a coating material, while with the continuous increase in the coating amount, the coating layer

may have become too thick, which in turn impedes Li-ion diffusion and ultimately leads to capacity degradation.

Figure 7a,b illustrate the EIS diagrams for NCM523, NCM523-LAF-1, and NCM523-LAF-Mg-Fe-1 samples, before and after the cycling process. At high frequencies, the curves display a semi-circular shape, suggestive of the charge transfer resistance (R_{ct}), meanwhile, at low frequencies, the curves reveal a straight line, representative of the Warburg impedance (W₀).^[31] The equivalent circuit diagram depicted in the figure is employed to fit the impedance data. Analysis using Zview2 software revealed that NCM523-LAF-Mg-Fe-1 exhibited the smallest R_{ct} values (65.05 Ω and 185.25 Ω) both before and after cycling, while the original NCM523 demonstrated the largest R_{ct} values (200.12 Ω and 453.35 Ω). After cycling, the R_{ct} of the pristine NCM523 increases sharply, indicating a thickening of the CEI due to electrolyte decomposition under high voltage, as well as the collapse of the surface structure of the active material. In contrast, the increase in R_{ct} for NCM523-LAF-Mg-Fe-1 is less pronounced, which can be attributed to the formation of stable ion-conducting channels by the Mg-Fe co-doped LAF coating. This reduces the direct contact between the electrolyte and the active material, thereby suppressing interfacial side reactions, such as transition metal dissolution. Moreover, although the pure LAF coating (NCM523-LAF-1) also reduced the R_{ct}, its post-cycling R_{ct} value of 385.95 Ω remained higher than that of the co-doped samples. This can be attributed to the fact that Mg-Fe co-doping not only expanded the lattice spacing of LAF, which enhances the Li⁺ diffusion rate, but also improved the electronic conductivity of the coating through modulation of the electronic structure, thereby more effectively reducing the interfacial impedance. This advantage significantly contributes to the superior electrochemical performance of the NCM523-LAF-Mg-Fe-1 sample. Furthermore, Figure S7, Supporting Information presents the fitted EIS curves for NCM523-LAF-Mg-1 and NCM523-LAF-Fe-1 before and after 200 cycles. The R_{ct} values before and after 200 cycles were 135.6 Ω vs 315.2 Ω and 102.3 Ω vs 356.6 Ω, respectively, both surpassing the corresponding values of the NCM523-LAF-Mg-Fe-1 electrode. This observation further substantiates that the LAF-Mg-Fe coating effectively reduced the R_{ct} measurements of the samples, thereby considerably enhancing the conductivity of the cathode materials. Figure 7c-e depicts the CV curves in the initial three cycles of the samples NCM523, NCM523-LAF-1, and NCM523-LAF-Mg-Fe-1. The voltage difference ΔE_p ($E_{pa} - E_{pc}$) between the oxidation and reduction peaks in the curve represents the degree of polarization of the electrode material during the cycling process. A larger difference denotes a more pronounced polarization of the electrode material.^[32] The potential differences between the oxidation and reduction peaks of NCM523, NCM523-LAF-1, and NCM523-LAF-Mg-Fe-1 were determined to be 0.220 V, 0.205 V, and 0.200 V, respectively. Notably, the co-doped sample (NCM523-LAF-Mg-Fe-1) exhibited the smallest voltage gap between the redox peaks, indicating that the modified coating effectively reduces polarization effects, thereby enhancing the electrochemical performance.

This study investigates the failure mechanisms and modification effects of the cycled NCM523, NCM523-LAF-1, and NCM523-LAF-Mg-Fe-1 electrodes extracted from coin cells, analyzed by

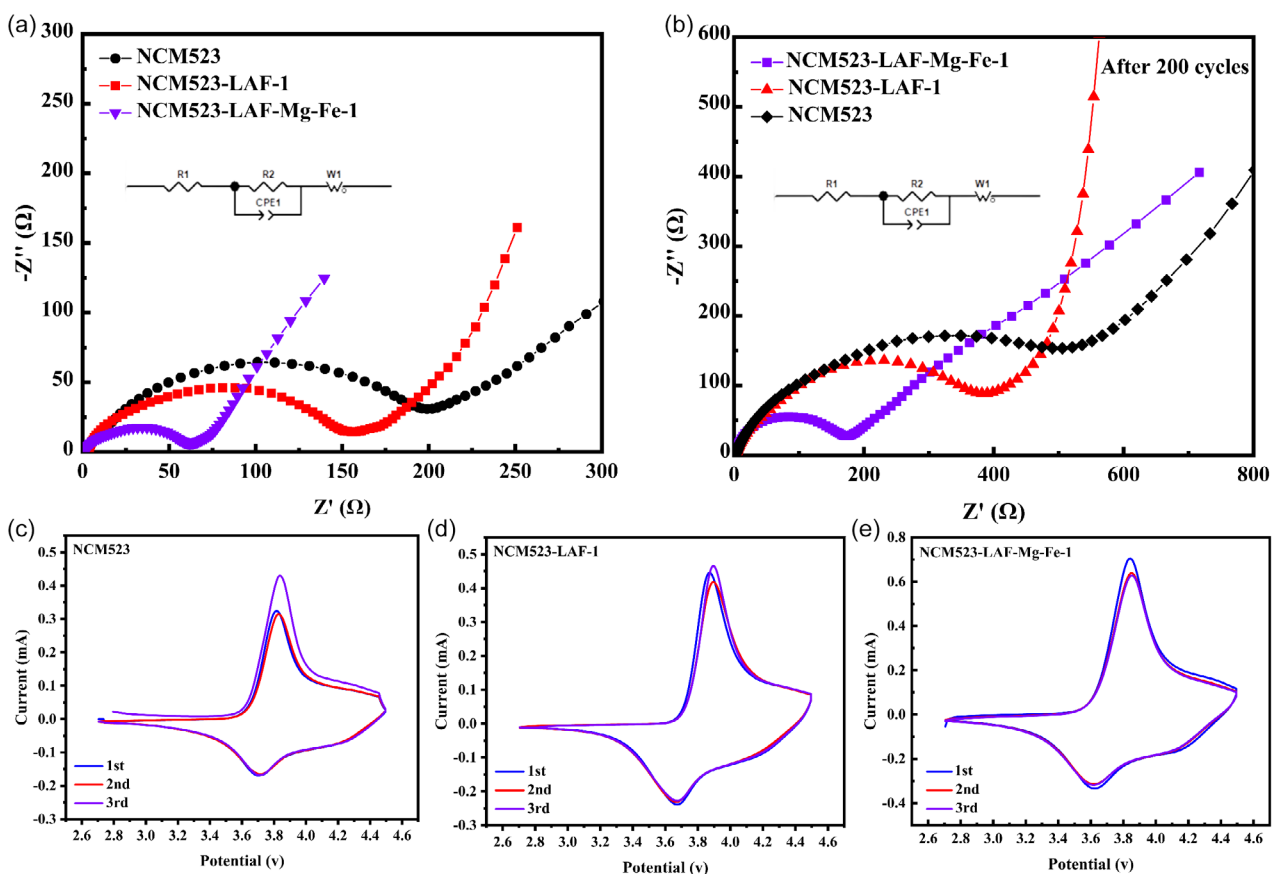


Figure 7. a) EIS spectra of NCM523, NCM523-LAF-1, and NCM523-LAF-Mg-Fe-1 before and b) after cycling. c) CV curves of NCM523. d) NCM523-LAF-1 and e) NCM523-LAF-Mg-Fe-1.

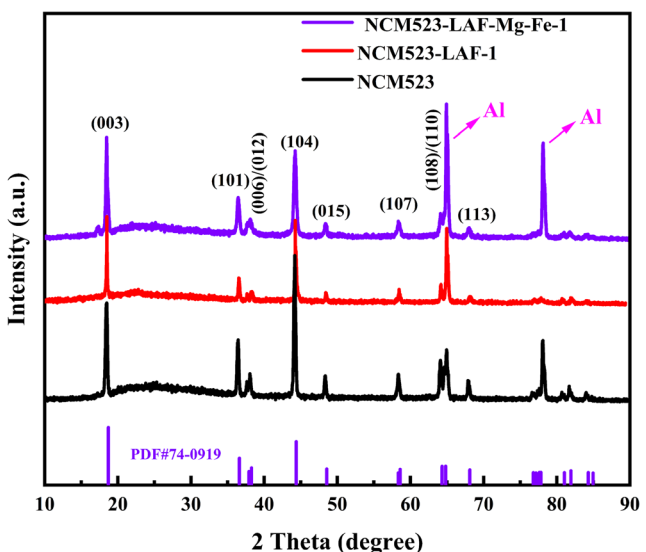


Figure 8. XRD results of NCM523, NCM523-LAF-1, and NCM523-LAF-Mg-Fe-1 samples after 200 cycles.

XRD and SEM. As presented in **Figure 8** and **Table 2**, the latter details the unit cell parameters and the $I(003)/I(104)$ intensity ratios for the three samples post-cycling. Notably, the $I(003)/I(104)$ ratios for both modified samples fall below 1.2, indicating

Table 2. The cell parameters of the bare NCM523, NCM523-LAF-1, and NCM523-LAF-Mg-Fe-1 samples after 200 cycles.

Sample	a [Å]	c [Å]	c/a	$I[003]/I[104]$
NCM523	2.87972	14.24324	4.94605	0.78
NCM523-LAF-1	2.87774	14.25801	4.95458	1.01
NCM523-LAF-Mg-Fe-1	2.87676	14.25997	4.95696	1.05

a significant increase in cation mixing. However, the $I(003)/I(104)$ value of NCM523-LAF-Mg-Fe-1 (1.05) remains higher than that of the NCM523 (0.78) and NCM523-LAF-1 (1.01) samples, suggesting that the LAF-Mg-Fe coating effectively mitigates the intensification of cation mixing during cycling. **Figure 9** displays the SEM images of NCM523, NCM523-LAF-1, and NCM523-LAF-Mg-Fe-1 samples after cycling, with Figure 9a,b corresponding to NCM523-LAF-Mg-Fe-1, Figure 9c,d to NCM523-LAF-1, and Figure 9e,f to NCM523. The images reveal that after 200 cycles, cracks are evident in the particles of both modified and unmodified NCM523, indicating that particle rupture and crack formation occur under high-voltage conditions. However, in comparison to the pure NCM523 and NCM523-LAF-1 samples, the modified NCM523-LAF-Mg-Fe-1 sample shows fewer surface cracks, demonstrating that the presence of the coating effectively reduces crack formation.

Figure 10 illustrates the mechanism by which Mg and Fe co-doped Li_3AlF_6 enhances the electrochemical performance of

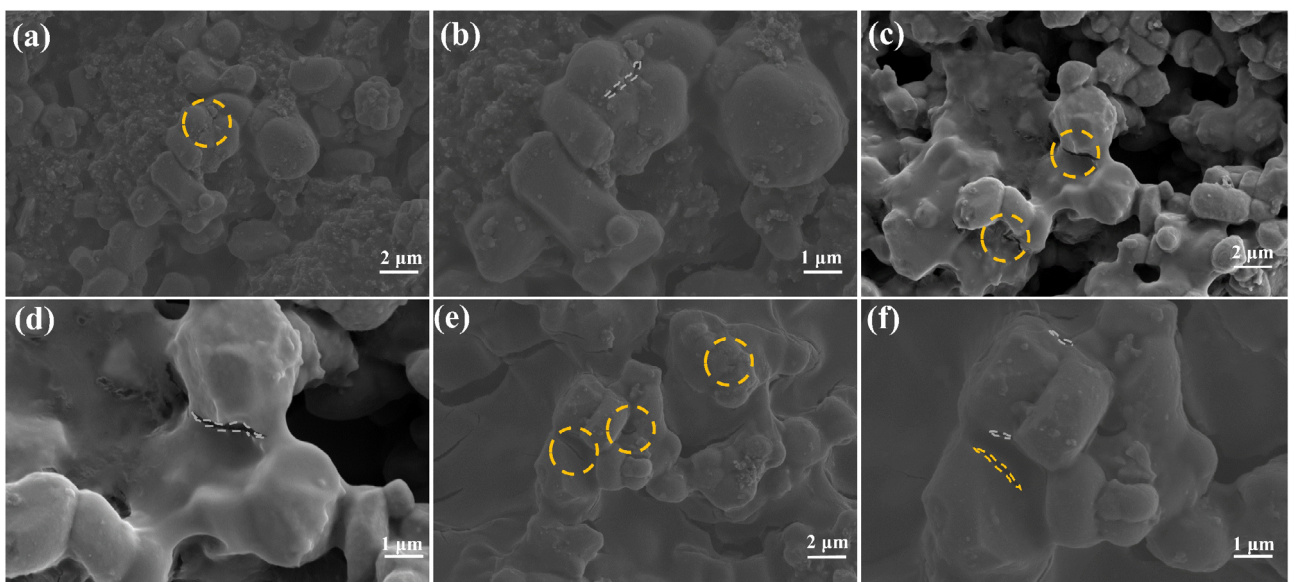


Figure 9. SEM micrographs and local magnification of a,b) NCM523-LAF-Mg-Fe-1 particles after 200 cycles. c,d) NCM523-LAF-1 particles after 200 cycles, and e,f) NCM523 particles after 200 cycles.

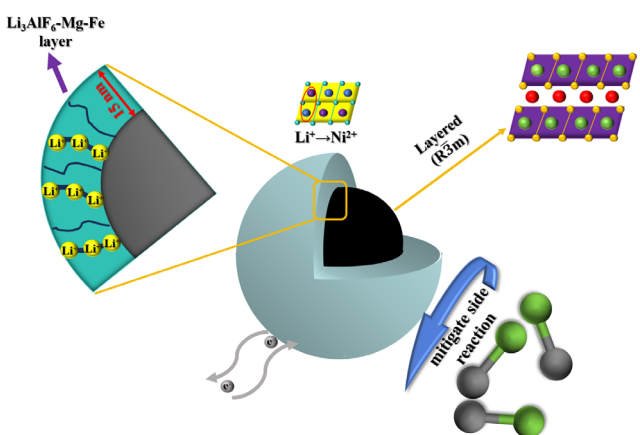


Figure 10. Schematic mechanism of Mg-Fe co-doped Li_3AlF_6 coating enhancing high-voltage stability of NCM523.

NCM523 as a surface modification coating. Firstly, the LAF-Mg-Fe coating on the surface of NCM523 hinders interactions with the electrolyte, thus lowering the chance of adverse reactions on the surface of NCM523. The modified material forms a stable and conductive surface layer, which significantly enhances lithium-ion and electron transport while effectively preventing irreversible phase transitions in NCM523 during cycling, thus improving its electrochemical efficiency compared to traditional Li_3AlF_6 coatings, which exhibit relatively low conductivity. Additionally, the coating stabilizes the lattice structure of NCM523 and mitigates cation mixing during high-voltage charge-discharge cycles.

3. Conclusion

In summary, the Mg-Fe co-doped Li_3AlF_6 -coated single-crystal NCM523 exhibits excellent electrochemical performance under

high-voltage conditions. The modified coating significantly enhances cycling performance by suppressing interfacial side reactions, mitigating electrolyte corrosion under high voltages, and inhibiting crack formation. Moreover, the incorporation of Mg and Fe further improves the ionic and electronic conductivity of the coating, thereby improving the material's rate capability. Additionally, post-cycling XRD and SEM analyses reveal that the coating maintains excellent morphological and structural stability even after high-voltage cycling. Overall, the Mg-Fe co-doped Li_3AlF_6 coating layer shows considerable promise as a high-voltage cathode coating material. This research introduces a potent method for enhancing the electrochemical performance of NCM materials when subjected to high-voltage environments, thus promoting the development of lithium-ion batteries characterized by higher energy density.

4. Experimental Section

Materials Synthesis

Single crystal NCM523 powder (2 g) (Ningbo Ronbay New Energy Technology Co. Ltd) was added to 100 mL of deionized water containing LiNO_3 , NH_4F , $\text{Al}(\text{NO}_3)_3 \cdot 9\text{H}_2\text{O}$, $\text{Fe}(\text{NO}_3)_3 \cdot 9\text{H}_2\text{O}$ and $\text{Mg}(\text{NO}_3)_2 \cdot 6\text{H}_2\text{O}$ (all of the aforementioned drugs are from Sinopharm Chemical Reagent Co. Ltd), the molar ratio of $\text{Al}(\text{NO}_3)_3 \cdot 9\text{H}_2\text{O}$, $\text{Fe}(\text{NO}_3)_3 \cdot 9\text{H}_2\text{O}$ and $\text{Mg}(\text{NO}_3)_2 \cdot 6\text{H}_2\text{O}$ is 0.96:0.02:0.02. The solution was stirred at 600 rpm using magnetic stirring at 80 °C for 6 h to ensure uniform coating. After centrifugation at 7000 rpm for 10 min, the precipitate was dried at 60 °C for 12 h. The obtained powder is subsequently positioned in a tube furnace and subjected to high-temperature calcination in a nitrogen atmosphere. The temperature for calcination was set at 400 °C, calcination was conducted for 6 h, and the heating rate was maintained at 5 °C/min. Finally, Mg-Fe double-doped Li_3AlF_6 -coated NCM523 cathode materials were prepared according to the mass percentages of 1 wt%, 2 wt%, and 3 wt%, named NCM523-LAF-Mg-Fe-1, NCM523-LAF-Mg-Fe-2, and NCM523-LAF-Mg-Fe-3, respectively. In addition,

for the sample with 1 wt% coating amount, only Mg (NO₃)₂·6H₂O or Fe (NO₃)₃·9H₂O was added in the process, and other synthesis conditions were not changed. The molar ratio of Al(NO₃)₃·9H₂O to Fe(NO₃)₃·9H₂O or Mg (NO₃)₂·6H₂O was 0.96:0.04, which was named NCM523-LAF-Fe-1 and NCM523-LAF-Mg-1, respectively, and samples without addition, which was named NCM523-LAF-1.

Materials Synthesis

The crystal structure of the synthesized material was analyzed using an X-ray diffractometer (XRD, D-max2500PC) at a scanning rate of 3°/min. The lattice parameters were analyzed through the General Structure Analysis System (GSAS) software. The samples were examined through scanning electron microscopy (SEM, SU8010, 2 kV) and transmission electron microscopy (TEM, JEM-2100 F) to evaluate their surface features and lattice arrangement. Furthermore, XPS (ESCALABX) was utilized to identify the types and compositions of the surface elements of the material.

Half-Cell Assembly and Electrochemical Test

Within a glove box purged with ultra-pure argon (ensuring oxygen and water levels remain below 0.01 mL m⁻³), CR2032 half-cells were constructed. Lithium metal sheet served as the anode, while Celgard-2400 polypropylene served as the separator. The electrolyte consisted of a 1M LiPF₆ solution combined with diethyl carbonate (DEC), ethylene carbonate (EC), and ethyl methyl carbonate (EMC) in equal proportions of 1:1:1. The preparation involved: the active material, along with the polyvinylidene fluoride (PVDF) and conductive agent (super-p), was blended into a uniform slurry using N-methyl-2-pyrrolidone (NMP) as the solvent, adhering to a mass ratio of active material to super-p to PVDF of 8:1:1. The obtained slurry was evenly applied to the aluminum foil, achieving a coating weight of 2.0–2.5 mg cm⁻². The material was dried in a vacuum oven for 12 h and subsequently sliced into discs with a diameter of 14 mm to function as the cathode material. The first discharge capacity, cycling stability, and rate performance of the materials were assessed with the LAND battery testing system (CT-3002 A). The electrochemical workstation (CHI 660 E) was utilized to acquire the cyclic voltammetry (CV) curves along with the electrochemical impedance spectroscopy (EIS) data. The lithium-ion diffusion coefficient was evaluated via the GITT method.

Acknowledgements

The authors gratefully acknowledge the financial support by the program of Science and Technology International Cooperation Project of Qinghai Province (No. 2022-HZ-811).

Conflict of Interest

The authors declare no conflict of interest.

Author Contributions

Boyu Liu: conceptualization (equal); data curation (lead); formal analysis (equal); investigation (equal); validation (equal); Visualization (equal); writing—original draft (equal). **Qing Pang:** conceptualization (equal); investigation (equal); methodology (equal). **Tengfei Wang:** project administration (equal); visualization (equal). **Xiufen Li:** data curation (supporting); project

administration (supporting); validation (supporting). **Hongyu Wang:** data curation (lead); formal analysis (equal); funding acquisition (equal); methodology (equal); project administration (equal); resources (equal); supervision (equal); validation (equal); visualization (equal); writing—review & editing (equal).

Data Availability Statement

The data that support the findings of this study are available from the corresponding author upon reasonable request.

Keywords: electrochemical performance · high voltage · Mg-Fe co-doped · single crystal NCM523

- [1] D. Andre, S.-J. Kim, P. Lamp, S. F. Lux, F. Maglia, O. Paschos, B. Stiaszny, *J. Mater. Chem. A* **2015**, *3*, 6709.
- [2] J. Langdon, A. Manthiram, *Energy Storage Mater.* **2021**, *37*, 143.
- [3] Z. Zhong, L. Chen, S. Huang, W. Shang, L. Kong, M. Sun, L. Chen, W. Ren, *J. Mater. Sci.* **2020**, *55*, 2913.
- [4] H. Dong, H. Wang, J. Qi, J. Wang, W. Ji, J. Pan, X. Li, Y. Yin, S. Yang, *ACS Sustainable Chem. Eng.* **2022**, *10*, 11587.
- [5] S. Klein, P. Bärmann, T. Beuse, K. Borzutzki, J. E. Frerichs, J. Kasnatscheew, M. Winter, T. Placke, *ChemSusChem* **2021**, *14*, 595.
- [6] Y. Zhang, Z. Wang, Y. Zhong, H. Wu, S. Li, Q. Cheng, P. Guo, *Ionics* **2021**, *27*, 13.
- [7] Y. Shi, M. Zhang, D. Qian, Y. S. Meng, *Electrochim. Acta* **2016**, *203*, 154.
- [8] J. Hao, Z. Yu, H. Liu, W. Song, J. Liu, L. Kong, C. Li, *J. Alloys Compd.* **2019**, *806*, 814.
- [9] X. Jiang, Z. Yuan, J. Liu, X. Jin, L. Jin, P. Dong, Y. Zhang, Y. Yao, Q. Cheng, C. Liu, *Int. J. Electrochem. Sci.* **2018**, *13*, 2341.
- [10] W. D. Richards, L. J. Miara, Y. Wang, J. C. Kim, G. Ceder, *Chem. Mater.* **2016**, *28*, 266.
- [11] B. Liu, D. Wang, M. Avdeev, S. Shi, J. Yang, W. Zhang, *ACS Sustainable Chem. Eng.* **2019**, *8*, 948.
- [12] R. Miyazaki, G. Yamaguchi, E. Yagi, T. Yoshida, T. Tomita, *Solid State Ionics* **2024**, *410*, 116549.
- [13] H. Kobayashi, G. Yuan, Y. Gambe, I. Honma, *ACS Appl. Energy Mater.* **2021**, *4*, 9866.
- [14] J. Xie, A. D. Sendek, E. D. Cubuk, X. Zhang, Z. Lu, Y. Gong, T. Wu, F. Shi, W. Liu, E. J. Reed, *ACS Nano* **2017**, *11*, 7019.
- [15] J. Qian, L. Liu, J. Yang, S. Li, X. Wang, H. L. Zhuang, Y. Lu, *Nat. Commun.* **2018**, *9*, 4918.
- [16] R. Dang, Y. Qu, Z. Ma, L. Yu, L. Duan, W. Lü, *J. Phys. Chem. C* **2021**, *126*, 151.
- [17] J. Yan, H. Huang, J. Tong, W. Li, X. Liu, H. Zhang, H. Huang, W. Zhou, *Interdiscip. Mater.* **2022**, *1*, 330.
- [18] Y.n. Hou, X. Li, W. Liu, H. Kou, H. M. K. Sari, X. Song, J. Li, S. Dou, X. Liu, S. Deng, *Mater. Today Energy* **2019**, *14*, 100353.
- [19] Y. Lv, X. Cheng, W. Qiang, B. Huang, *J. Power Sources* **2020**, *450*, 227718.
- [20] Y. Li, C. Wan, Y. Tian, J. Li, C. Yang, W. Zhang, X. Zhang, Z. Hao, Z. Yang, P. Guo, *Appl. Surf. Sci.* **2023**, *609*, 155162.
- [21] Y. Huang, H. Zhu, H. Zhu, J. Zhang, Y. Ren, Q. Liu, *Nanotechnol.* **2021**, *32*, 295701.
- [22] Y.-h. Luo, Q.-l. Pan, H.-x. Wei, Y.-d. Huang, L.-b. Tang, Z.-y. Wang, C. Yan, J. Mao, K.-h. Dai, Q. Wu, *Mater. Today* **2023**, *69*, 54.
- [23] F. Friedrich, B. Strehle, A. T. Freiberg, K. Kleiner, S. J. Day, C. Erk, M. Piana, H. A. Gasteiger, *J. Electrochem. Soc.* **2019**, *166*, A3760.
- [24] N. D. Rodrigo, C. Jayawardhana, B. L. Lucht, *J. Electrochem. Soc.* **2022**, *169*, 030519.
- [25] L. Dahéron, R. Dedryvère, H. Martinez, M. Ménétrier, C. Denage, C. Delmas, D. Gonbeau, *Chem. Mater.* **2008**, *20*, 583.
- [26] K. Park, J.-H. Park, S.-G. Hong, J. Yoon, S. Park, J.-H. Kim, D. Yoon, H. Kim, Y.-H. Son, J.-H. Park, *Electrochim. Acta* **2016**, *222*, 830.
- [27] J. Hu, K. Chen, C. Li, *ACS Appl. Mater. Interfaces* **2018**, *10*, 34322.

- [28] J. Billaud, D. Sheptyakov, S. Sallard, D. Leanza, M. Talianker, J. Grinblat, H. Sclar, D. Aurbach, P. Novák, C. Villevieille, *J. Mater. Chem. A* **2019**, *7*, 15215.
- [29] T. Sattar, S.-H. Lee, S.-J. Sim, B.-S. Jin, H.-S. Kim, *Int. J. Hydrogen Energy* **2020**, *45*, 19567.
- [30] X. Fan, Y. Liu, X. Ou, J. Zhang, B. Zhang, D. Wang, G. Hu, *Chem. Eng. J.* **2020**, *393*, 124709.
- [31] C. Liang, L. Liu, Z. Jia, C. Dai, Y. Xiong, *Electrochim. Acta* **2015**, *186*, 413.
- [32] A. V. Ivanishchev, I. A. Ivanishcheva, S. Lee, J.-J. Kim, Y.-J. Kim, C. Bae, S.-C. Nam, J.-H. Song, *J. Electroanal. Chem.* **2023**, *950*, 117864.

Manuscript received: April 9, 2025
Revised manuscript received: May 19, 2025
Version of record online:
